Andreev tunneling through a double quantum-dot system coupled to a ferromagnet and a superconductor: Effects of mean-field electronic correlations

E. C. Siqueira* and G. G. Cabrera†
Instituto de Física "Gleb Wataghin," UNICAMP, CP 6165, Campinas 13083-970, SP, Brazil
(Received 17 August 2009; revised manuscript received 7 February 2010; published 30 March 2010)

We study the transport properties of a hybrid nanostructure composed of a ferromagnet, two quantum dots, and a superconductor connected in series. By using the nonequilibrium Green's function approach, we have calculated the electric current, the differential conductance, and the transmittance for energies within the superconductor gap. In this regime, the mechanism of charge transmission is the Andreev reflection, which allows for a control of the current through the ferromagnet polarization. We have also included interdot and intradot interactions, and have analyzed their influence through a mean-field approximation. In the presence of interactions, Coulomb blockade tend to localize the electrons at the double-dot system, leading to an asymmetric pattern for the density of states at the dots, and thus reducing the transmission probability through the device. In particular, for nonzero polarization, the intradot interaction splits the spin degeneracy, reducing the maximum value of the current due to different spin-up and spin-down densities of states. Negative differential conductance appears for some regions of the voltage bias, as a result of the interplay of the Andreev scattering with electronic correlations. By applying a gate voltage at the dots, one can tune the effect, changing the voltage region where this novel phenomenon appears. This mechanism to control the current may be of importance in technological applications.

DOI: 10.1103/PhysRevB.81.094526 PACS number(s): 74.45.+c, 73.63.Kv, 73.23.Hk, 74.78.Na

I. INTRODUCTION

The interest in transport properties of mesoscopic systems has increased a lot due to their potential for present and future technologies. Recent advances in the experimental development of nanostructures are mainly aimed at the study of purely quantum phenomena and effects based on electron-spin properties (*spintronics*). In particular, hybrid resonant structures composed by one or more quantum dots (QDs) coupled to normal (N), ferromagnetic (F), and superconductor (S) metals have been studied.[1–8] In systems composed by one quantum dot, electron-spin properties have been extensively explored. In the special case of junctions composed by a ferromagnet and a superconductor it is possible to construct spin valves which control the current flow through those systems. Andreev reflection (AR) permits such control, by varying the polarization of the ferromagnet attached to the system, as shown in several papers.[9–15] AR (Ref. 16) is a mechanism in which a Cooper pair is formed in the superconductor from the combination of an incident electron coming from the normal metal with energy ω and spin σ, with another electron with energy $-\omega$ and spin $-\sigma$. Both electrons enter the superconductor as a Cooper pair, leaving a reflecting hole in the ferromagnetic electrode. Andreev states are located within the superconductor gap, where no quasiparticles states are available.

In this work we have studied the transport properties of a hybrid nanostructure composed by a ferromagnet, two quantum dots,[14,17–22] and a superconductor connected in series (F-QD$_a$-QD$_b$-S). The addition of an extra quantum dot will allow us to study the interplay of electron correlations at the dots (for both intradot and interdot interactions), with the Andreev current. Figure 1 shows a schematic diagram of the system. The superconductor chemical potential is fixed to zero ($\mu_S=0$) and the bias is applied to the ferromagnetic electrode. There are also applied gate voltages at the dots a and b, namely, V_{ga} and V_{gb}, respectively. By using the nonequilibrium Green's function,[9,23–25] we have calculated the current (I), differential conductance (dI/dV), Andreev transmittance (T_{AR}), and the local density of states (LDOS) at the dots. All quantities are calculated for energies within the superconducting gap, the relevant range for the Andreev reflection, as functions of the voltage bias. We have also included intradot and interdot Coulomb correlations at the dots, and have analyzed its influence on the electric current through a mean-field approximation. In solids, both correlations compete to form charge or spin modulated structures. Those symmetry broken states are not possible in finite systems, as it is the case in our double-dot sample.[26] However, dot a is coupled to a ferromagnet, which breaks spin symmetry and dot b is coupled to a superconductor, which acts as a charge reservoir. Thus, interesting effects are expected, when the electronic interactions at the dots are taken into account. In this paper, those effects are displayed by the differential conductance, which shows asymmetric regions of negative values as a function of the applied bias, when the $I\times V$ characteristics are obtained. Negative differential conductance (NDC) have been observed in hybrid nanostructures composed by normal metals,[27] semiconductor-based devices,[28]

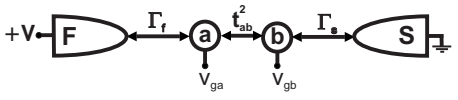

FIG. 1. Schematic showing the system studied in this work. The dot coupled to the ferromagnet electrode (F) is called a, and b is the one coupled to the S. The superconductor has its chemical potential fixed to zero and the voltage bias is applied to the ferromagnet. Gate voltages are also applied at the dots. The different couplings are also indicated in the figure.

and more recently in molecular Josephson junctions.[29] There are also some theoretical studies on the NDC effect in those systems, using models beyond the mean-field approximation.[30–36] In our work, electron interactions at the dots are treated within a mean-field approach. This approximation, plus additional correlations introduced through couplings to the F/S electrodes, gives rise to NDC effects. For Andreev currents, correlation parameters at the dots are limited by the size of the superconductor gap.

This paper is organized as follows: in Sec. II we present the model under consideration and derive the transport properties by using the nonequilibrium Green's functions. In Sec. III the numerical results are presented and discussed. Some conclusions are given in Sec. IV.

II. MODEL AND FORMULAS

A. Hamiltonian

The system displayed in Fig. 1 is described by the following Hamiltonian:

$$\mathcal{H} = \mathcal{H}_{\mathrm{F}} + \mathcal{H}_{\mathrm{S}} + \mathcal{H}_{dqd} + \mathcal{H}_{T},$$

$$\mathcal{H}_{\mathrm{F}} = \sum_{k\sigma} (\epsilon_k - \sigma h - \mu_{\mathrm{F}}) a^{\dagger}_{k\sigma} a_{k\sigma},$$

$$\mathcal{H}_{\mathrm{S}} = \sum_{p\sigma} \epsilon_p s^{\dagger}_{p\sigma} s_{p\sigma} + \sum_{p} [\Delta s^{\dagger}_{p\uparrow} s^{\dagger}_{-p\downarrow} + \mathrm{H.c.}],$$

$$\hat{\mathcal{H}}_{dqd} = \sum_{\sigma} E_{a\sigma} \hat{n}_{a\sigma} + \sum_{\sigma} E_{b\sigma} \hat{n}_{b\sigma}, \tag{1}$$

where

$$E_{a\sigma} = eV_{ga} + \frac{\mathcal{K}}{2}\langle \hat{n}_b \rangle + \frac{\mathcal{U}}{2}\langle \hat{n}_{a\bar{\sigma}} \rangle, \tag{2}$$

$$E_{b\sigma} = eV_{gb} + \frac{\mathcal{K}}{2}\langle \hat{n}_a \rangle + \frac{\mathcal{U}}{2}\langle \hat{n}_{b\bar{\sigma}} \rangle,$$

$$\mathcal{H}_T = \sum_{k\sigma} [t_f a^{\dagger}_{k\sigma} c_{a\sigma} + \mathrm{H.c.}] + \sum_{p\sigma} [t_s s^{\dagger}_{p\sigma} c_{b\sigma} + \mathrm{H.c.}] + \sum_{\sigma} [t_{ab} c^{\dagger}_{a\sigma} c_{b\sigma} + \mathrm{H.c.}]. \tag{3}$$

$\mathcal{H}_{\mathrm{F}}$ is the Hamiltonian of the F described by the Stoner model. The spin bands of F are shifted by h, the exchange energy. The ferromagnet chemical potential is fixed by the applied bias, i.e., $\mu_{\mathrm{F}}=eV$. $\mathcal{H}_{\mathrm{S}}$ is the Hamiltonian for a BCS superconductor with chemical potential fixed to zero as the ground, $\mu_{\mathrm{S}}=0$, and Δ being the superconducting gap. $\mathcal{H}_{dqd}$ is the Hamiltonian for the quantum dots in the mean-field approximation, which permits an exact equation for the self-energy. The energies $E_{a\sigma}$ and $E_{b\sigma}$ are renormalized by the interactions $\mathcal{K}$ (interdot) and $\mathcal{U}$ (intradot). The interactions also couple the renormalized energy levels with the mean occupations $\langle \hat{n}_a \rangle$ and $\langle \hat{n}_b \rangle$. In addition, it is included a gate voltage at the quantum dots a and b, namely, V_{ga} and V_{gb}, respectively. $\mathcal{H}_T$ is the Hamiltonian which describes all the tunneling processes: between dot a and the ferromagnet, with amplitude t_f, between dots with amplitude t_{ab}, and between dot b and the superconductor, with amplitude t_s.

We have not considered the occurrence of the Kondo resonance at the dots. While the Kondo effect has been experimentally observed in semiconducting quantum dots, coupling the dot to a ferromagnetic electrode will split the dot level, leading to the suppression of the Kondo effect.[37,38] Electron pairing in the superconductor electrode also competes with Kondo through the proximity effect.[20] Now, a discussion about the relative magnitude of the correlation parameters is in order. In this paper, $\mathcal{U}$ and $\mathcal{K}$ are limited to the gap value since we analyzed the contribution of a pure Andreev current (subgap current). This also restricts the voltages to very small values, typically on the order of mV or smaller. Our study is then confined to the weak correlation regime.

B. Green's functions

To calculate the transport properties we have used the nonequilibrium Green's function method.[9,23–25] All the physical quantities can be cast in terms of the Green's function of the dots. By using the Nambu 4×4 notation the retarded Green´s functions of the quantum dots are given by

$$\mathbf{G}^{r}_{aa} = \mathbf{G}^{r0}_{aa} + \mathbf{G}^{r}_{aa}\mathbf{t}^{\dagger}_{ab}\mathbf{G}^{r0}_{bb}\mathbf{t}_{ab}\mathbf{G}^{r0}_{aa}, \tag{4}$$

$$\mathbf{G}^{r}_{bb} = \mathbf{G}^{r0}_{bb} + \mathbf{G}^{r}_{bb}\mathbf{t}^{\dagger}_{ab}\mathbf{G}^{r0}_{aa}\mathbf{t}_{ab}\mathbf{G}^{r0}_{aa} \tag{5}$$

with

$$\mathbf{G}^{r0}_{aa} = \mathbf{g}^{r}_{aa}(1 - \Sigma^{r}_{\mathrm{F}}\mathbf{g}^{r}_{aa})^{-1}, \tag{6}$$

$$\mathbf{G}^{r0}_{bb} = \mathbf{g}^{r}_{bb}(1 - \Sigma^{r}_{\mathrm{S}}\mathbf{g}^{r}_{bb})^{-1}. \tag{7}$$

In these equations $\mathbf{G}^{r}_{aa}$ is the Green's function of the quantum dot a; $\mathbf{G}^{r}_{bb}$ is the Green's function of the quantum dot b; $\mathbf{g}^{r}_{aa}$ and $\mathbf{g}^{r}_{bb}$ are the Green's functions of the dots a and b isolated from the electrodes; $\mathbf{t}_{ab}$ describes the coupling between the dots; and $\mathbf{\Sigma}^{r}_{\mathrm{F}}$ and Σ^{r}_{S} are the retarded self-energies which describe the coupling of the dots with the superconductor and ferromagnet electrodes, respectively. Explicitly these self-energies are written as

$$\mathbf{\Sigma}^{r,a}_{\mathrm{F}}(\omega) = \mp \frac{i}{2}\begin{bmatrix} \Gamma_{f\uparrow} & 0 & 0 & 0 \\ 0 & \Gamma_{f\downarrow} & 0 & 0 \\ 0 & 0 & \Gamma_{f\downarrow} & 0 \\ 0 & 0 & 0 & \Gamma_{f\uparrow} \end{bmatrix} \tag{8}$$

with $\Gamma_{f\sigma}=2\pi|t_f|^2N_\sigma$ is the coupling strength, with t_f being the tunneling amplitude and N_σ the density of states for the ferromagnet spin σ band; and

$$\mathbf{\Sigma}_{\mathrm{S}}^{r,a}(\omega) = \mp \frac{i}{2}\Gamma_s \rho(\omega) \begin{bmatrix} 1 & -\frac{\Delta}{\omega} & 0 & 0 \\ -\frac{\Delta}{\omega} & 1 & 0 & 0 \\ 0 & 0 & 1 & \frac{\Delta}{\omega} \\ 0 & 0 & \frac{\Delta}{\omega} & 1 \end{bmatrix}, \tag{9}$$

where $\Gamma_s = 2\pi|t_s|^2 N_s$, with N_s being the density of states of the superconductor in the normal state and ρ_s is the modified BCS density of states $\rho(\omega) \equiv \frac{|\omega|\theta(|\omega|-\Delta)}{\sqrt{\omega^2-\Delta^2}} + \frac{\omega\theta(\Delta-|\omega|)}{i\sqrt{\Delta^2-\omega^2}}$, with the imaginary part accounting for Andreev states within the gap.[9,39]

Besides the retarded and advanced Green's functions, it is necessary to obtain the Keldysh Green's functions, which are calculated by the equation of motion technique. Since it is used a mean-field approximation for the interaction, the result for this Green's function is exact. The equation obtained for the Keldysh Green's function of dot a is given by

$$\mathbf{G}_{aa}^{<}(\omega) = \mathbf{G}_{aa}^{r}(\omega)\mathbf{\Sigma}_{T}^{<}(\omega)\mathbf{G}_{aa}^{a}(\omega) \tag{10}$$

with the "lesser" self-energy $\mathbf{\Sigma}_{T}^{<}$,

$$\mathbf{\Sigma}_{T}^{<}(\omega) = \mathbf{\Sigma}_{\mathrm{F}}^{<}(\omega) + \mathbf{t}_{ab}^{\dagger}\mathbf{G}_{bb}^{r0}\mathbf{\Sigma}_{S}^{<}(\omega)\mathbf{G}_{bb}^{a0}(\omega)\mathbf{t}_{ab}. \tag{11}$$

Correspondingly, the Keldysh equation for quantum dot b is given by

$$\mathbf{G}_{bb}^{<}(\omega) = \mathbf{G}_{bb}^{r}(\omega)\mathbf{\Sigma}_{Tb}^{<}(\omega)\mathbf{G}_{bb}^{a}(\omega) \tag{12}$$

with the lesser self-energy $\mathbf{\Sigma}_{Tb}^{<}$,

$$\mathbf{\Sigma}_{Tb}^{<}(\omega) = \mathbf{\Sigma}_{\mathrm{S}}^{<}(\omega) + \mathbf{t}_{ab}\mathbf{G}_{aa}^{r0}\mathbf{\Sigma}_{\mathrm{F}}^{<}(\omega)\mathbf{G}_{aa}^{a0}(\omega)\mathbf{t}_{ab}^{\dagger}. \tag{13}$$

The lesser self-energy for the ferromagnet electrode is given by

$$\mathbf{\Sigma}_{\mathrm{F}}^{<}(\omega) = i \begin{bmatrix} f_{\mathrm{F}}\Gamma_{f\uparrow} & 0 & 0 & 0 \\ 0 & \bar{f}_{\mathrm{F}}\Gamma_{f\downarrow} & 0 & 0 \\ 0 & 0 & f_{\mathrm{F}}\Gamma_{f\downarrow} & 0 \\ 0 & 0 & 0 & \bar{f}_{\mathrm{F}}\Gamma_{f\uparrow} \end{bmatrix} \tag{14}$$

in which $f_{\mathrm{F}} = f(\omega - eV)$ and $\bar{f}_{\mathrm{F}} = (\omega + eV)$ are the Fermi functions for electrons and holes, respectively.

The lesser self-energy for the superconductor electrode is given by

$$\mathbf{\Sigma}_{\mathrm{S}}^{<}(\omega) = if\Gamma_s \tilde{\rho}(\omega) \begin{bmatrix} 1 & -\frac{\Delta}{\omega} & 0 & 0 \\ -\frac{\Delta}{\omega} & 1 & 0 & 0 \\ 0 & 0 & 1 & \frac{\Delta}{\omega} \\ 0 & 0 & \frac{\Delta}{\omega} & 1 \end{bmatrix}, \tag{15}$$

where $f_{\mathrm{S}} = f(\omega)$ is the Fermi function for the superconductor electrode and $\tilde{\rho} = \frac{|\omega|}{\sqrt{\omega^2-\Delta^2}}$ is the conventional BCS density of states.

Equation (11) shows that the dot a, which is coupled to the ferromagnetic electrode on its left side, "sees" on its right side an effective electrode as a result of the interplay of dot b with the superconductor. Equation (13) can be interpreted in similar terms for dot b, with a "bare" superconductor electrode on the right side and an effective electrode on the left, resulting from the interaction of dot a with the ferromagnet. Since the superconductor and the ferromagnet present different band structures, there is an intrinsic asymmetry in this system which manifests itself in the transport properties.

C. Physical quantities

The Green's functions of the last section, calculated by the equation of motion method, permit to determine all the physical quantities necessary to analyze the transport properties of the F-QD$_a$-QD$_b$-S system. Since the interaction couples the dot levels through the mean occupation, as shown by Eqs. (2) and (3), it is necessary to perform a self-consistent calculation to determine the occupation at the dots first. Then, one can proceed to calculate the physical quantities of interest. In the following we show the expressions we have used to compute the LDOS, the current, the transmittance, and the mean occupation.

1. Local density of states

The LDOS of the quantum dots comes from the matrix elements (Refs. 11 and 33) of the retarded Green's function matrix (electron components in Nambu space). The LDOS for dots a and b are, respectively,

$$\text{LDOS-A} = -\frac{1}{\pi}\mathrm{Im}[G_{aa,11}^{r} + G_{aa,33}^{r}], \tag{16}$$

$$\text{LDOS-B} = -\frac{1}{\pi}\mathrm{Im}[G_{bb,11}^{r} + G_{bb,33}^{r}]. \tag{17}$$

2. Transmittance and current

Since the current is conserved, it can be calculated at any point of the circuit. Here, we choose to calculate the current at the ferromagnetic electrode, as the temporal variation in the number of electrons, i.e.,

$$I = -e\left\langle \frac{d\hat{N}_F}{dt} \right\rangle,$$

where $\hat{N}_F = \Sigma_{k\sigma} a^{\dagger}_{k\sigma} a_{k\sigma}$. By using the Heisenberg equation and the definition of the lesser Green's function of the dot a, it is possible to write the current as follow:

$$I = \frac{e}{\hbar}\int d\omega [\mathbf{G}^r_{aa}(\omega)\mathbf{\Sigma}^<_F(\omega) + \mathbf{G}^<_{aa}(\omega)\mathbf{\Sigma}^a_F(\omega) + \text{H.c.}]_{11+33}, \tag{18}$$

where the index 11+33 indicates a sum over the electron components in the Nambu space matrix. By substituting the matrix elements, the current can be cast to the following form:

$$I = \frac{e}{h}\int d\omega A(\omega)(f_F - \bar{f}_F). \tag{19}$$

In this work we only consider Andreev transport for energies within the superconductor gap. Thus, the current amplitude corresponding to the contribution of quasiparticles tunneling is zero.

The expression for the amplitude $A(\omega)$ is given by

$$A = \Gamma_{f\uparrow}(|G^r_{aa,14}|^2\Gamma_{f\uparrow} + |G^r_{aa,12}|^2\Gamma_{f\downarrow}) + \Gamma_{f\downarrow}(|G^r_{aa,34}|^2\Gamma_{f\uparrow} + |G^r_{aa,32}|^2\Gamma_{f\downarrow}).$$

The transmittance is obtained from the current formula,

$$T_{AR} = \frac{1}{2}[\Gamma_{f\uparrow}(|G^r_{aa,14}|^2\Gamma_{f\uparrow} + |G^r_{aa,12}|^2\Gamma_{f\downarrow}) + \Gamma_{f\downarrow}(|G^r_{aa,34}|^2\Gamma_{f\uparrow} + |G^r_{aa,32}|^2\Gamma_{f\downarrow})]. \tag{20}$$

3. Self-consistent calculations

Since the Green's functions are dependent on the mean occupations via Eqs. (2) and (3), it is necessary to calculate those quantities at the dots. From the definition of the lesser Green's function, one straightforwardly obtains the system of equations below

$$\langle n_{a\uparrow}\rangle = \frac{1}{2\pi i}\int_{-\infty}^{+\infty} G^<_{aa,11}(\omega),$$

$$\langle n_{a\downarrow}\rangle = \frac{1}{2\pi i}\int_{-\infty}^{+\infty} G^<_{aa,33}(\omega),$$

$$\langle n_{b\uparrow}\rangle = \frac{1}{2\pi i}\int_{-\infty}^{+\infty} G^<_{bb,11}(\omega),$$

$$\langle n_{b\downarrow}\rangle = \frac{1}{2\pi i}\int_{-\infty}^{+\infty} G^<_{bb,33}(\omega).$$

These integral equations have to be solved numerically in a self-consistent way. Once the occupation numbers are obtained, it is possible to calculate the other physical quantities. Results are shown below.

III. RESULTS AND DISCUSSION

Next, we present the results obtained from numerical calculations. First, we show the LDOS at the quantum dots in the absence of electronic correlations. We investigate the effects of the different couplings of the model, i.e., the coupling between dots and the coupling of the dots with the leads. In the following sections, we discuss the role of the interactions. All examples displayed for the latter case correspond to finite polarization of the ferromagnet, thus keeping our results on safe ground when using mean-field approximations. We use the $P=0.3$ and 0.8 cases as prototypes, being this range typical of most well known and used ferromagnetic leads.[40] We analyze separately the effects of the interactions. The interdot interaction $\mathcal{K}$ breaks the LDOS symmetry at the dots, changing the position and amplitude of resonances. As a result, we find the NDC effect for a range of values of parameters. The intradot interaction $\mathcal{U}$ lifts the spin degeneracy, as can be seen by the splitting of the differential conductance and LDOS peaks. In the final section, we present results when both interactions, $\mathcal{K}$ and $\mathcal{U}$, are active and are of the same order of magnitude. The interplay of both magnitudes leads to the NDC phenomenon in some range of the bias. This voltage region can be controlled and tuned by application of gate voltages at the dots.

A. Noninteracting case

In this section, the LDOS of the quantum dots is described without interactions. This permits us to analyze the resonance structure presented by these quantities, which plays a central role in all transport properties, including the interacting case as well. The system is asymmetric since the ferromagnetic left electrode is modeled with a continuous density of states while the superconductor electrode, on the right side, presents a gap for quasiparticles states, with a complex density of states within the gap, corresponding to evanescent Andreev states, responsible for the Copper pair conversion at the interface.

Figure 2 shows the LDOS at the dots, for different values of the interdot coupling (electron hopping between dots) t_{ab}, in units of the superconducting gap. For $t_{ab}=0.02$, the dots are almost decoupled from each other. As a result, features of the density of states mainly reflect the coupling with the electrodes. LDOS for dot a presents one peak centered in $\omega=0$ with a finite width. The broadening results from the hybridization of the dot level with the ferromagnetic band. There is a finite probability for the electron to escape from the dot to the electrode. On the other hand, LDOS-B presents two sharp symmetrical peaks. This resonant structure represents the hybridization between the dot level with the Andreev states. The peaks correspond to the electron and hole channels, as expected from the BCS model for the superconductor electrode.

As the coupling between the dots is increased, two additional peaks at the center emerge for both LDOS, as observed in the examples for $t_{ab}=0.30$ and 0.46. These peaks come from the resonance between the discrete dot levels. For LDOS-B, the intensity of the Andreev peaks decay with the dot coupling.

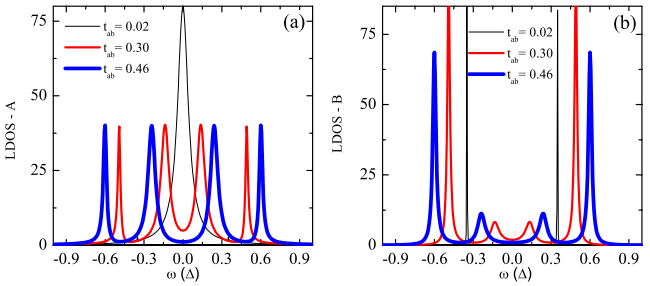

FIG. 2. (Color online) LDOS for different values of coupling between dots, t_{ab}. Fixed parameters: Γ_f=0.1, Γ_s=1.0, P=0, k_BT =0.01, and eV_{ga}=eV_{gb}=0. (a) LDOS for QD a, coupled to the ferromagnet. For t_{ab}=0.02, the LDOS is dominated by the coupling with the ferromagnet, revealed by the broadening of the central peak. By increasing t_{ab}, the resonances from the superconductor (external peaks) and from interdot coupling (central peaks) appear. (b) LDOS for QD b, coupled to the superconductor. For t_{ab}=0.02 the LDOS is dominated by the coupling with the superconductor, as displayed by the equidistant peaks around ω=0; these peaks are the Andreev resonances. By increasing t_{ab}, the interdot coupling peaks (central peaks) appear in addition to the Andreev resonances. All parameters are expressed in units of the superconductor gap.

The effect of the coupling with the superconductor is illustrated by the LDOS curves shown in Fig. 3. When the interaction with the superconductor is weak Γ_s=0.05, both LDOS present a two-peak structure resulting from the interdot coupling (t_{ab}=0.5 in the examples shown). When the coupling with the superconductor is increased, the Andreev peaks appear and are more intense in LDOS-B.

The effect on the LDOS by varying the coupling with ferromagnetic electrode is shown in Fig. 4. When the coupling with the ferromagnet is increased, the discrete structure of the LDOS is transformed into a continuum of states, as a result of the hybridization of the discrete dot levels with the continuous band of the ferromagnet. Internal peaks almost disappear for $\Gamma_f > 0.5$.

Isolated quantum dots present one level degenerate in spin. When coupled to each other with t_{ab}, there is an admixture of them, resulting in a bonding and an antibonding levels, in analogy with a H_2 molecule.[26] In our model, those levels corresponds to the central peaks of the LDOS. When the electrodes are attached to the double-dot system, the above peaks broaden and two additional peaks appear corresponding to the superconducting Andreev states. By tuning the parameters of the model, it is possible to change the number of peaks, their widths and the distance between them, which in turn can be used to control the current.

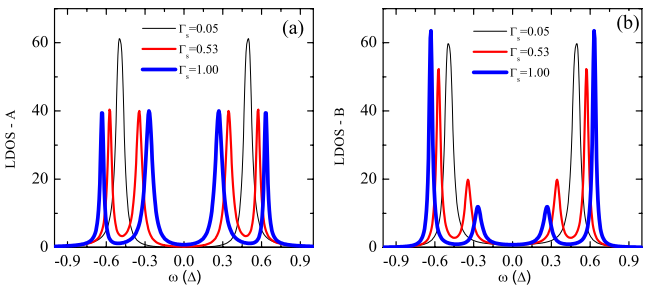

FIG. 3. (Color online) LDOS for different values of the coupling with the superconductor, Γ_s. Fixed parameters: Γ_f=0.1, t_{ab}=0.5, P=0, k_BT=0.01, and eV_{ga}=eV_{gb}=0. (a) LDOS for quantum dot a, coupled to the ferromagnet. (b) LDOS for quantum dot b, coupled to the superconductor. The distinct behavior of LDOS-A and LDOS-B is explained by the stronger coupling of b with S. The increase in the coupling with S results in a bigger separation between the resonance peaks. All parameters are expressed in units of the superconductor gap.

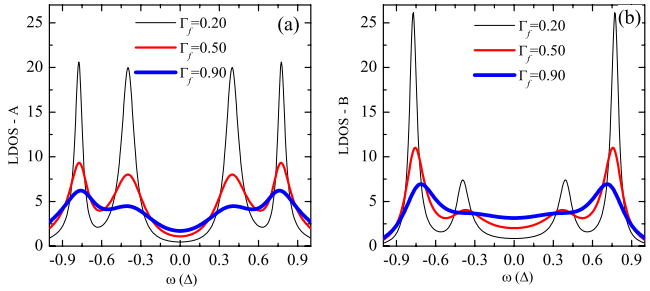

FIG. 4. (Color online) LDOS for different values of coupling with the ferromagnet, Γ_f. Fixed parameters: Γ_s=1.0, t_{ab}=0.5, P =0, k_BT=0.01, and eV_{ga}=eV_{gb}=0. (a) LDOS for quantum dot a, coupled to the ferromagnet. (b) LDOS for quantum dot b, coupled to superconductor. By increasing Γ_f, the density of states presents a broader pattern, displaying an admixture between the ferromagnetic energy band and the hybridized states of the dots. All parameters are expressed in units of the superconductor gap.

B. Interacting case: Interdot interaction

In Fig. 5(a) we plot some $I \times V$ characteristics for different values of the interdot interaction $\mathcal{K}$. These curves show a plateau pattern which is due to the peak structure of the

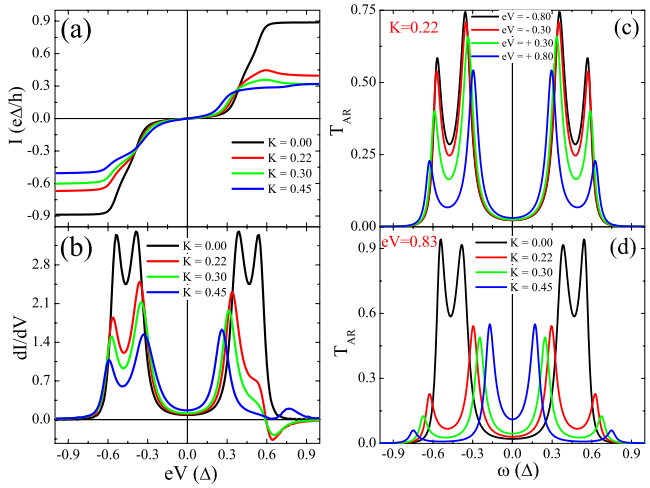

FIG. 5. (Color online) (a) current (I) versus applied bias (V) for some values of interdot interaction. (b) Corresponding differential conductance, showing regions of negative values. (c) Andreev transmittance (T_{AR}) for some values of applied bias for $\mathcal{K}$=0.22. (d) Andreev transmittance (T_{AR}) for some values of $\mathcal{K}$, for applied bias eV=0.83. Fixed parameters: Γ_f=0.19, Γ_s=0.40, t_{ab}=0.5, P=0.3, $\mathcal{U}$=0, k_BT=0.01, and eV_{ga}=eV_{gb}=0. All parameters are expressed in units of the superconductor gap.

LDOS at the quantum dots. When the interaction is increased, the plateau value is reduced, ranging from $I=0.90$ for $\mathcal{K}=0$ to $I=0.30$ for $\mathcal{K}=0.45$, since higher values of the interaction implies a stronger Coulomb repulsion between dots. But for small voltages ($eV<0.30$), we observe an unusual behavior, where the trend is inverted, although this is a tiny effect. In Fig. 5(b), we plot the corresponding differential conductance, which allow for a better resolution of the $I\times V$ curves. The symmetric structure for $\mathcal{K}=0$ is broken when $\mathcal{K}\neq 0$, the asymmetry being more pronounced the higher the values of $\mathcal{K}$. For some examples of the figure, NDC in the characteristics is found around $\mathcal{K}=0.6$. From our numerical calculations, NDC effects are present in the range $0.08<\mathcal{K}<0.4$. For $\mathcal{K}$ greater than 0.4, NDC is suppressed and a positive peak emerges in dI/dV, as can be seen in the example for $\mathcal{K}=0.45$.

From these results, we conclude that the mechanism of the NDC is not linearly related to the Coulomb blockade effect. The interaction plays a more subtle role in changing the transmittance of the system. In fact, looking at the differential conductance, we note that when increasing $\mathcal{K}$, the second peak for positive bias is suppressed. Thus, for some values of $\mathcal{K}$ there is a suppression of some of the resonant peaks and this causes an additional reduction in the transmittance for some values of the applied bias. This effect causes the differential conductance to assume negative values. The Andreev transmittance is displayed in Figs. 5(c) and 5(d). There is a variation with the applied bias, in contrast to the noninteracting case. The interaction couples the occupation number at the dots, which implies a nontrivial dependence of the transmittance with the applied bias. In Fig. 5(c), we plot the transmittance for $\mathcal{K}=0.22$, for some values of the applied bias. There is a reduction in the amplitude with the increase in the bias but the spectrum is symmetric with respect to ω. In Fig. 5(d), we show the transmittance at fixed bias $eV=0.83$, for various values of $\mathcal{K}$. There is a reduction in the transmittance and a shift of the peaks, however the variation is not systematic, as shown by the example for $\mathcal{K}=0.45$, which does not follow the trend of the other values. Reduction in the transmittance with increasing bias is one of the causes of NDC. However, the absence of NDC for negative bias strongly hints that there are additional ingredients to explain the phenomenon. One important factor is the asymmetry in the LDOS, which appears when the interaction $\mathcal{K}$ is turned on. In Figs. 6(a) and 6(b), we show the effect of the interaction on the peak structure of the LDOS at the dots. The symmetric shape seen in Figs. 2–4 is lost when the interaction is included. By increasing the interaction toward the gap value, some peaks are suppressed (one central and one external) and other are reinforced (one central and one external), the LDOS presenting a more localized character. Central peaks of the LDOS are associated to states resonating between dots while external peaks are the channels for the Andreev reflection. The symmetry is critical to allow electronic transfer through the structure since the sum of the energies of the electrons available to form a Cooper pair have to be equal to the chemical potential of the superconductor (which is zero). Thus, the Andreev current is optimized when the LDOS peaks are symmetric and the suppression of one of them causes an effective reduction in the current, with the emergence of the NDC effect.

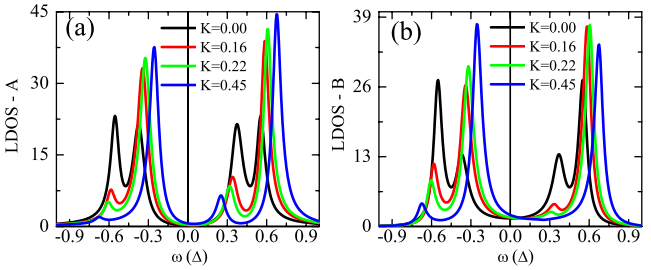

FIG. 6. (Color online) LDOS for different values of interdot interaction. Fixed parameters: $\Gamma_f=0.19$, $\Gamma_s=0.40$, $t_{ab}=0.5$, $P=0.3$, $\mathcal{U}=0$, $k_BT=0.01$, $eV=+0.62$, and $eV_{ga}=eV_{gb}=0$. (a) LDOS for quantum dot a, coupled to ferromagnet. (b) LDOS for quantum dot b, coupled to superconductor. In both, the interaction introduces an asymmetry which is related to the NDC effect. All parameters are expressed in units of the superconductor gap.

When a negative bias is applied to the ferromagnetic electrode, its chemical potential is reduced in relation to the superconductor's one. Thus, the current is established by extracting Cooper pairs from superconductor electrode. Those electrons, with antiparallel spins, fill the lower energy states available at the dots, so only the peaks of the negative frequency branch of the LDOS will participate in the conduction process. This is the explanation for the absence of NDC for negative bias in the $I\times V$ characteristics, as shown in Fig. 5(a).

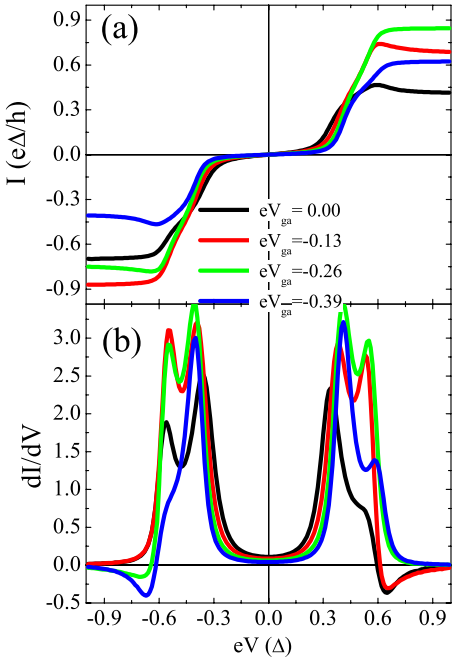

FIG. 7. (Color online) Current and differential conductance vs applied bias for some values of the gate voltage at dot a. Fixed parameters: $\Gamma_f=0.2$, $\Gamma_s=0.4$, $t_{ab}=0.50$, $P=0.3$, $\mathcal{K}=0.22$, $\mathcal{U}=0$, $k_BT=0.01$, and $V_{gb}=0$. (a) Current versus applied bias: the gate potential modifies the current profile appearing some regions of NDC in both, negative and positive values of the applied bias. (b) Differential conductance for the corresponding $I\times V$ curves. All parameters are expressed in units of the superconductor gap.

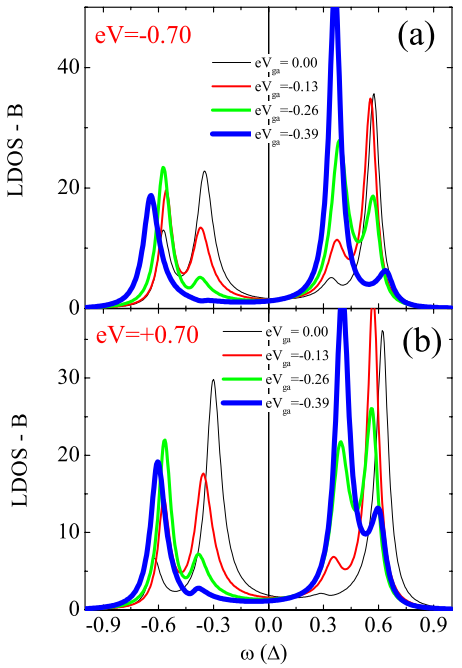

FIG. 8. (Color online) LDOS of dot b vs electron energy for some values of the gate voltage at dot a. Fixed parameters: $\Gamma_f=0.2$, $\Gamma_s=0.4$, $t_{ab}=0.50$, $P=0.3$, $k_BT=0.01$, $V_{gb}=0$, $\mathcal{K}=0.22$, and $\mathcal{U}=0$. (a) LDOS-B for applied bias $eV=-0.70$. The second peak for negative energy is progressively suppressed and vanishes at $eV_{ga}=-0.39$. (b) LDOS-B for applied bias $eV=+0.70$. The first peak for positive energy, that was absent for $eV_{ga}=0$, emerges with application of the gate voltage. All parameters are expressed in units of the superconductor gap.

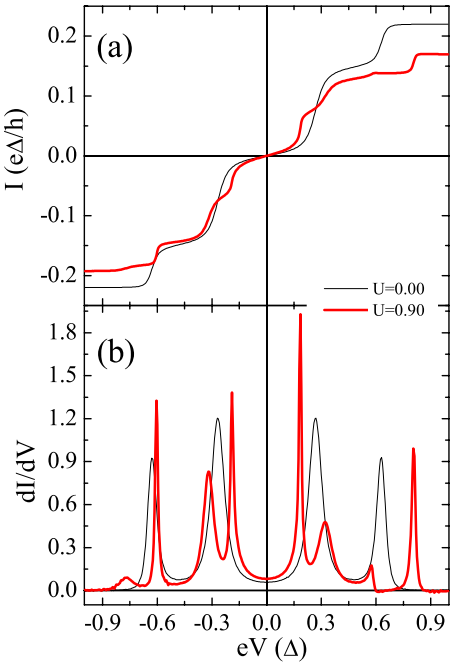

FIG. 9. (Color online) Current and differential conductance vs applied bias for some values of the intradot interaction. Fixed parameters: $\Gamma_f=0.1$, $\Gamma_s=1.00$, $t_{ab}=0.50$, $P=0.80$, $\mathcal{K}=0$, $k_BT=0.01$, and $eV_{ga}=eV_{gb}=0$. (a) Current vs applied bias. (b) Differential conductance. The intradot interaction lifts the spin degeneracy, producing a splitting of the peaks in the dI/dV curves. Very different values of Γ_f and Γ_s have been used in the example to get a larger separation between the resonance peaks. All parameters are expressed in units of the superconductor gap.

Next, to show that the NDC effect originates from the asymmetry of the LDOS, we have recalculated the $\mathcal{K}=0.22$ case of Fig. 5 but now applying a gate voltage at dot a while keeping the gate voltage at the other dot fixed and equal to $\mu_S=0$. The results are qualitatively similar if the gate potential at dot b is varied while the one at a is kept fixed and equal to μ_S. As shown in Figs. 7(a) and 7(b), the NDC appears for negative values of the applied bias, for V_{ga} approximately ranging from -0.26 to -0.39. In the range $-0.13<V_{ga}<+0.13$, the NDC appears for positive bias. To make contact with the asymmetry of the LDOS at the dots, in Figs. 8(a) and 8(b), we plot the LDOS-B for values of the bias at the neighborhood of the NDC, namely, $eV=-0.70$ and $+0.70$. The LDOS-A presents a similar behavior. By tuning the gate voltage V_{ga}, we can change the amplitude and position of the peaks in the LDOS. Eventually, some of the peaks vanish, resulting in NDC effect. The above figures corroborate the role of the LDOS in the appearance of the NDC regions. In fact, peaks of the LDOS and transmittance are resonances resulting from the coupling between the dots and the electrodes. As shown in Figs. 5 and 6, the interdot interaction affects the LDOS and the transmittance in a way similar to "destructive interference," changing the position and amplitude of the peaks. One can tune such "destructive interference," by introducing a gate voltage, thus modifying the values of bias where NDC takes place, as shown in Fig. 8. This process of controlling the current through the device may be important for practical applications.

C. Interacting case: Intradot interaction

Next, we present mean-field results that include the intradot (onsite) interaction $\mathcal{U}$, with no interdot repulsion ($\mathcal{K}=0$). As shown in Eqs. (2) and (3), the intradot interaction splits the up-spin and down-spin states at each quantum dot, with the corresponding splitting of the transmittance and differential conductance peaks. However, as indicated by Eqs. (2) and (3), this effect can only be observed for different up-spin and down-spin occupations. This condition is met for nonzero values of the polarization P of the ferromagnet, when different numbers of spin-up and spin-down electrons are injected to the dots. The rates at which electrons are injected are $\Gamma_{f\uparrow}/h=\Gamma_f(1+P)/h$ and $\Gamma_{f\downarrow}/h=\Gamma_f(1-P)/h$ for spin up and down, respectively. In Fig. 9 the $I\times V$ characteristics and the corresponding differential conductance are shown for different values of the intradot interaction. As long as $\mathcal{U}\neq 0$, the peaks start to split and for $\mathcal{U}=0.90$ the differential conductance presents a clear pattern with eight peaks. The $I\times V$ characteristic, for $\mathcal{U}=0.90$, also shows a number of additional steps and a final plateau with a reduced value of the current. The reduction in the maximum value of the current with P is explained by the reduction in the available conducting channels, as discussed in Ref. 41. Since the current is established by Andreev reflection, it is necessary an equal number of spin-up and spin-down electrons to form Cooper pairs. Since the density of states for spin down is smaller, the current is limited by the number of spin-down electrons.

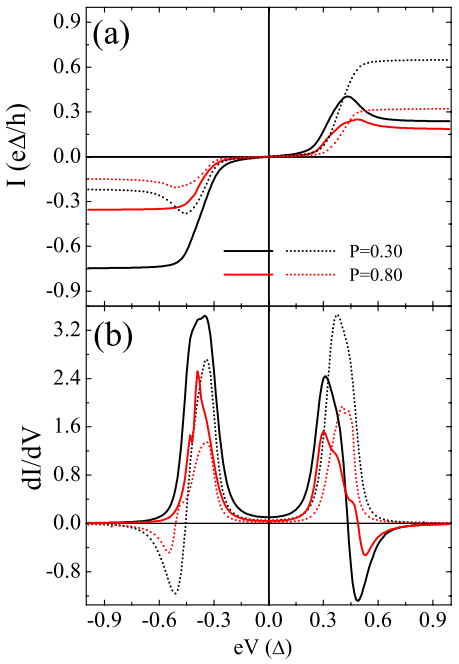

FIG. 10. (Color online) Current and differential conductance vs applied bias for different values of the ferromagnet polarization. Solid lines: $V_{ga}=V_{gb}=-0.13$. Dotted lines: $V_{ga}=-0.39$ and $V_{gb}=-0.10$. Fixed parameters: $\Gamma_f=0.20$, $\Gamma_s=0.26$, $t_{ab}=0.40$, $\mathcal{K}=0.25$, $\mathcal{U}=0.25$, and $k_BT=0.01$. (a) Current vs applied bias. (b) Differential conductance. The increase in the polarization suppresses NDC by reducing the available states in the conduction process. All parameters are expressed in units of the superconductor gap.

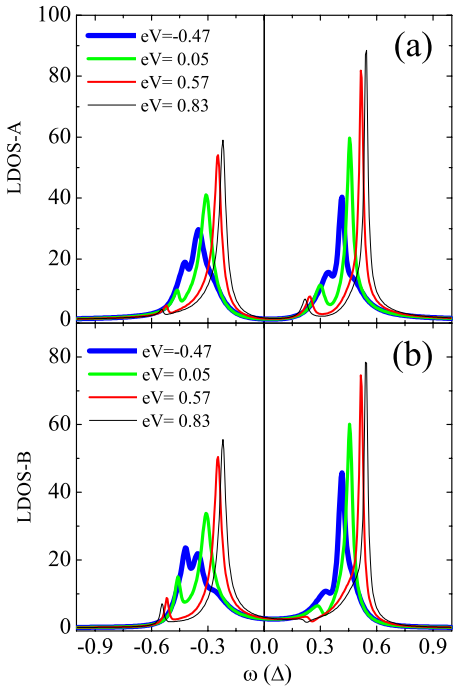

FIG. 11. (Color online) Corresponding LDOS for some values of the applied bias. By adjusting the hopping t_{ab} and the coupling with superconductor Γ_s, it is possible to reduce the peaks of the LDOS allowing to observe the NDC even at high values of the polarization. Fixed parameters: $P=0.80$, $\Gamma_f=0.20$, $\Gamma_s=0.26$, $t_{ab}=0.40$, $\mathcal{K}=0.25$, $\mathcal{U}=0.25$, $k_BT=0.01$, and $V_{ga}=V_{gb}=-0.13$. (a) LDOS for dot a, coupled to ferromagnet. (b) LDOS for dot b, coupled to superconductor. All parameters are expressed in units of the superconductor gap.

In the examples presented in Fig. 9, which corresponds to $P=0.80$, NDC effects are absent. By increasing the polarization the NDC region is reduced and eventually disappears when we further increase the polarization. The mechanism that accounts for the NDC effect for intradot interaction is the same as the one presented in the previous sections: the reduction in the transmittance with the applied bias, combined with asymmetries of the LDOS. For values of the polarization of $\approx 0.80-0.90$, the mean number of electrons participating in the conduction is so reduced that a further reduction in the channels does not imply in a reduction in the electrical current. This is the cause of the absence of NDC in the examples of Fig. 9.

D. Interaction case: Intradot and Interdot interactions

In the previous sections we have presented results when one of the interactions is absent. However, it is possible to obtain the NDC effect when both interactions are active. In Fig. 10 we show $I\times V$ characteristics for $\mathcal{U}=\mathcal{K}=0.25$. In spite of the high polarization values, $P=0.30$ and 0.80, there are regions of voltage with the NDC effect in all the examples. For $eV_{ga}=eV_{gb}=-0.13$ (solid curves), NDC appears for applied bias $eV\gtrsim 0.48$. For $V_{ga}=-0.39$ and $V_{gb}=-0.10$ the NDC appears for negative bias $eV\lesssim -0.48$ (dotted curves). Comparing with Fig. 9, besides the different values for the interactions and gate voltages, the coupling constants t_{ab} and Γ_s have been modified. In fact, by changing the coupling constants and the bias, it is possible to suppress some peaks of the LDOS and the current will be sensitive to this reduction in the channels, even for polarization values close to unity. In this case, the NDC effect can be recovered. An example is shown in Fig. 11, where the LDOS is plotted for $P=0.80$ and $eV_a=eV_b=-0.13$. For the parameters chosen, the LDOS present a four-peak structure. When we increase the applied bias there is a suppression of the first and third peaks while the second and fourth are enhanced. The suppression is almost complete for the first peak of the LDOS at dot a and for the third peak at dot b. As a result, the Andreev current decreases with increasing voltage (NDC effect) since Andreev reflection requires a symmetric pair of channels in order to conduct.

IV. CONCLUSION

In this work, we have studied the effects of the interdot and intradot interactions on the transport properties of a double quantum-dot system coupled to a ferromagnet and a superconductor. Energy parameters of the theory are limited by the size of the superconductor gap. This way, the conduction through the device is controlled by Andreev scattering processes (subgap current). In the first part of the paper, the role of the coupling between dots and the couplings between dots and leads were elucidated. Next, we study the effects of

electronic correlations at the dots within a mean-field approximation. For both interactions, interdot and intradot, we found regions of voltage with NDC. The NDC effect is a typical phenomenon in resonant tunneling spectroscopy, and since the pioneering work of Chang *et al.*,[42] it has been recognized as fundamental for practical applications, such as amplifiers, switching devices, and high-frequency oscillators. Differently from one-electron-tunneling resonances, for the Andreev current we need electron and hole states of opposite spins symmetrically located around the chemical potential. Thus, symmetry and lack of symmetry of the LDOS at the dots play an important role for Andreev reflection processes. Correlations tend to localize the electrons at the double-dot system, changing the LDOS by suppressing some peaks, shifting their positions, and lifting spin degeneracy, leading to an asymmetric pattern of the LDOS. This asymmetry reduces the number of available states to conduct through the Andreev reflection mechanism. By changing the polarization of the ferromagnet, one can also change the relative spin populations entering the two-dot system. The above phenomena, combined with the bias dependence of the transmittance, produce the NDC effect for some regions of the applied voltage. Through the gate voltages, one can tune the effect and change the bias region where NDC appears.

Such kind of devices, as the one considered here, are on the verge of being produced by present technology and our theoretical study may be useful to control the current in practical applications. $\mathcal{K}$, $\mathcal{U}$, and P are intrinsic parameters, which are sample dependent. However, the NDC effect can be tuned by the gate voltages, as shown in this contribution. With the addition of a second ferromagnetic electrode, one may open channels for crossed Andreev reflections, with the control of the current by the relative polarization directions of the two ferromagnets.

A final comment on the validity of the mean-field approximation is in order. Results as those shown in Figs. 10 and 11 were obtained at finite values of the polarization and gate voltages. Under the above conditions, mean-field results can sensibly capture the physics involved and one can regard the predicted NDC effects as bona fide phenomena. Mean-field approximations are known to be extremely useful in providing a proper qualitative picture and their real range of validity usually extrapolates the theoretical predictions. However, the exact extension of the validity of the approximation can only be addressed by experiments.

ACKNOWLEDGMENTS

The authors acknowledge partial support from the Brazilian agency Conselho Nacional de Desenvolvimento Científico e Tecnológico (CNPq).

*ecosta@ifi.unicamp.br
†cabrera@ifi.unicamp.br

[1] W. G. van der Wiel, S. De Franceschi, J. M. Elzerman, T. Fujisawa, S. Tarucha, and L. P. Kouwenhoven, Rev. Mod. Phys. **75**, 1 (2002).
[2] I. Žutić, J. Fabian, and S. Das Sarma, Rev. Mod. Phys. **76**, 323 (2004).
[3] R. Hanson, L. P. Kouwenhoven, J. R. Petta, S. Tarucha, and L. M. K. Vandersypen, Rev. Mod. Phys. **79**, 1217 (2007).
[4] S. Das Sarma, J. Fabian, X. Hu, and I. Zutic, Solid State Commun. **119**, 207 (2001).
[5] W. Z. Shangguan, T. C. Au Yeung, Y. B. Yu, and C. H. Kam, Phys. Rev. B **63**, 235323 (2001).
[6] Z. Chen, B. Wang, D. Y. Xing, and J. Wang, Appl. Phys. Lett. **85**, 2553 (2004).
[7] Q.-f. Sun, J. Wang, and T. H. Lin, Phys. Rev. B **59**, 3831 (1999).
[8] J.-F. Feng, X.-S. Wu, and S.-S. Jiang, J. Appl. Phys. **99**, 08F713 (2006).
[9] Z. Y. Zeng, B. Li, and F. Claro, Phys. Rev. B **68**, 115319 (2003).
[10] H.-Y. Song and S.-P. Zhou, Phys. Lett. A **372**, 6773 (2008).
[11] G. Deutscher and D. Feinberg, Appl. Phys. Lett. **76**, 487 (2000).
[12] X. F. Cao, Y. Shi, X. Song, S. Zhou, and H. Chen, Phys. Rev. B **70**, 235341 (2004).
[13] J.-F. Feng and S.-J. Xiong, Phys. Rev. B **67**, 045316 (2003).
[14] Y.-X. Li, H.-Y. Choi, H.-W. Lee, and J.-J. Liu, J. Appl. Phys. **101**, 103918 (2007).
[15] Y. Zhu, Q.-f. Sun, and T. H. Lin, Phys. Rev. B **65**, 024516 (2001).
[16] A. F. Andreev, Zh. Eksp. Teor. Fiz. **46**, 1823 (1964) [Sov. Phys. JETP **19**, 1228 (1964)].
[17] L. Hofstetter, S. Csonka, J. Nygard, and C. Schonenberger, Nature (London) **461**, 960 (2009).
[18] J.-L. Li and Y.-X. Li, J. Phys.: Condens. Matter **20**, 465202 (2008).
[19] H. Pan and T.-H. Lin, Phys. Rev. B **74**, 235312 (2006).
[20] F. S. Bergeret, A. Levy Yeyati, and A. Martín-Rodero, Phys. Rev. B **74**, 132505 (2006).
[21] Y.-X. Li, H.-W. Lee, and H.-Y. Choi, Phys. Lett. A **372**, 6424 (2008).
[22] R. Hornberger, S. Koller, G. Begemann, A. Donarini, and M. Grifoni, Phys. Rev. B **77**, 245313 (2008).
[23] L. V. Keldysh, Zh. Eksp. Teor. Fiz. **47**, 1515 (1964) [Sov. Phys. JETP **20**, 1018 (1965)].
[24] A.-P. Jauho, N. S. Wingreen, and Y. Meir, Phys. Rev. B **50**, 5528 (1994).
[25] J. Rammer and H. Smith, Rev. Mod. Phys. **58**, 323 (1986).
[26] L. M. Falicov and R. A. Harris, J. Chem. Phys. **51**, 3153 (1969).
[27] K. Ishibashi, M. Suzuki, T. Ida, and Y. Aoyagi, Appl. Phys. Lett. **79**, 1864 (2001).
[28] W. Song, E. E. Mendez, V. Kuznetsov, and B. Nielsen, Appl. Phys. Lett. **82**, 1568 (2003).
[29] P. Makk, S. Csonka, and A. Halbritter, Phys. Rev. B **78**, 045414 (2008).
[30] J. Fransson and O. Eriksson, Phys. Rev. B **70**, 085301 (2004).
[31] J. Fransson and O. Eriksson, J. Phys.: Condens. Matter **16**, L85 (2004).
[32] G. A. Lara, P. A. Orellana, and E. V. Anda, Phys. Rev. B **78**, 045323 (2008).

[33] J. N. Pedersen, B. Lassen, A. Wacker, and M. H. Hettler, Phys. Rev. B **75**, 235314 (2007).
[34] H. W. Liu, T. Fujisawa, T. Hayashi, and Y. Hirayama, Phys. Rev. B **72**, 161305(R) (2005).
[35] V. H. Nguyen, V. L. Nguyen, and P. Dollfus, Appl. Phys. Lett. **87**, 123107 (2005).
[36] A. Zazunov, D. Feinberg, and T. Martin, Phys. Rev. B **73**, 115405 (2006).
[37] J. Martinek, Y. Utsumi, H. Imamura, J. Barnaś, S. Maekawa, J. König, and G. Schön, Phys. Rev. Lett. **91**, 127203 (2003).
[38] J. Martinek, M. Sindel, L. Borda, J. Barnaś, J. König, G. Schön, and J. von Delft, Phys. Rev. Lett. **91**, 247202 (2003).
[39] G. E. Blonder, M. Tinkham, and T. M. Klapwijk, Phys. Rev. B **25**, 4515 (1982).
[40] R. J. Soulen *et al.*, Science **282**, 85 (1998).
[41] M. J. M. de Jong and C. W. J. Beenakker, Phys. Rev. Lett. **74**, 1657 (1995).
[42] L. L. Chang, L. Esaki, and R. Tsu, Appl. Phys. Lett. **24**, 593 (1974).